ELSEVIER

On trapdoor faulting at Sierra Negra volcano, Galápagos

Sigurjón Jónsson[a,*], Howard Zebker[b], Falk Amelung[c]

[a]*Institute of Geophysics, ETH Hönggerberg, CH-8093 Zürich, Switzerland*
[b]*Geophysics Department, Stanford University, Stanford, CA 94305, USA*
[c]*Division of Marine Geology and Geophysics - RSMAS, University of Miami, 4600 Rickenbacker Causeway, Miami, FL 33149, USA*

Abstract

Rapid uplift observed during 1992–1997 at Sierra Negra volcano, western Galápagos, was followed by deformation that we have previously interpreted as trapdoor faulting on an intra-caldera fracture system. At that time, no direct evidence for the trapdoor faulting was available to support this interpretation. Here we report field evidence of recent faulting at Sierra Negra and provide direct measurements of the faulting using pixel offsets between satellite radar amplitude (backscatter) images. Our field observations, carried out in 2001, indicate that recent faulting occurred along the southern part of the intra-caldera fault system with maximum offset of at least 0.5–1 m. Differences between two satellite radar amplitude images show 1.4 ± 0.2 m range change across this fault system. This suggests that 1.5 ± 0.2 m of faulting occurred, assuming vertical ground displacements, consistent with our previous modeling results. Results of numerical modeling indicate that growing sills can cause faulting of the intrusion roof on outward-dipping or nearly vertical faults. This occurs at high excess magma pressure when the lateral extent (half-length) of the sill becomes greater than its depth. The derived ~2-km deep Sierra Negra sill exhibits trapdoor faulting ~3 km south of the center of the sill. Therefore, these modeling results provide a plausible mechanical explanation for the trapdoor fault at Sierra Negra.
© 2004 Elsevier B.V. All rights reserved.

1. Introduction

The Galápagos archipelago is located on the Nazca plate about 1000 km west of Ecuador, just south of the east–west-trending Galápagos spreading center (Fig. 1a). The islands are a collection of about 20 basaltic shield volcanoes that progressively become younger towards the west due to the eastward motion of the Nazca plate (Christie et al., 1992). Unlike Hawaiian volcanoes, they do not have well-developed rift zones, but instead are characterized by steep slopes, large summit calderas, a pattern of arcuate vents near the caldera rims, and radial vents further away on the flanks (Chadwick and Howard, 1991; Chadwick and Dieterich, 1995).

* Corresponding author. Fax: +41 44 633 1065.
E-mail addresses: sj@erdw.ethz.ch (S. Jónsson),
zebker@stanford.edu (H. Zebker), amelung@rsmas.miami.edu
(F. Amelung).
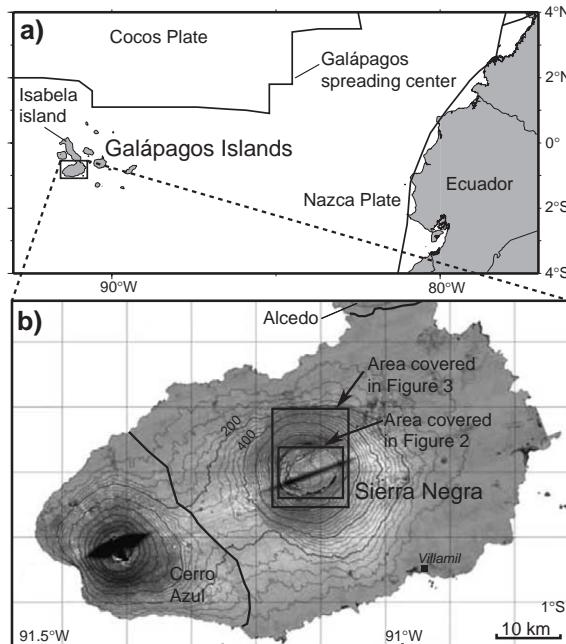
Fig. 1. (a) The Galápagos archipelago is on the Nazca plate, just south of the Galápagos spreading center between the Cocos and Nazca plates. (b) Sierra Negra volcano is located on southern Isabela island, between Cerro Azul and Alcedo volcanoes, black lines indicate approximate boundaries between the volcanoes (after Reynolds et al., 1995). The topographic information is from a TOPSAR digital elevation model (Mouginis-Mark et al., 1996) with contour lines drawn every 40 m (thicker lines every 200 m). Missing elevation information appears as dark elongated areas across Cerro Azul and Sierra Negra calderas. Rectangles mark areas shown in Figs. 2 and 3.

Sierra Negra volcano, located on southern Isabela island, is the most voluminous volcano in the western Galápagos. It is 60 km long and 40 km wide subaerially with a height of 1140 m (Fig. 1). The Sierra Negra caldera is larger (7 km×10 km), but also shallower (110 m deep), than other calderas in the western Galápagos (Reynolds et al., 1995; Munro and Rowland, 1996). Eleven historical eruptions have occurred on Sierra Negra since 1813 (Simkin and Siebert, 1994). The last eruption took place in 1979 after a 16-year hiatus, producing a large lava flow (0.9 km³) on the north flank of the volcano (Reynolds et al., 1995). Most of the recent eruptions have produced lavas on the north flank, while intra-caldera lava flows are older, estimated at 1000–3000 years (Reynolds et al., 1995).

Geodetic interferometric synthetic aperture radar (InSAR) observations exhibit spatially and temporally variable uplift on Sierra Negra during 1992–1999 (Amelung et al., 2000). The maximum line-of-sight (LOS) displacement during this time was 2.5 m in the center of the caldera, which corresponds to 2.7 m uplift. During 1992–1997 and during 1998–1999 the uplift is consistent with a shallow inflating sill with maximum uplift in the center of the caldera. Inflation during 1997–1998, however, was markedly asymmetric with maximum uplift occurring near south facing intra-caldera normal faults that bound an elevated inner-caldera floor. The interpretation in our earlier study was that uplift prior to 1997 caused extension of the caldera floor, eventually leading to trapdoor faulting on the intra-caldera faults sometime in 1997–1998 (Amelung et al., 2000). However, no field observations or other direct measurements were available to constrain the age and amount of faulting.

In this article we re-investigate trapdoor faulting at Sierra Negra volcano using new measurements of the faulting. We begin by describing the intra-caldera fault system and the caldera structure. We then review crustal deformation observations from 1992 to 2002 and our previous modeling results. We strengthen our initial InSAR-based interpretation of trapdoor faulting

using two different methods. First, we report evidence of recent faulting along the intra-caldera faults, observed during fieldwork in January 2001, and second, we use synthetic aperture radar (SAR) amplitude image range offsets to measure directly the displacement across the faults. Finally, we offer an explanation on why trapdoor faulting may be occurring in the caldera of Sierra Negra volcano.

2. Intra-caldera faults on Sierra Negra volcano

The summit caldera of Sierra Negra volcano is relatively shallow in comparison to other western Galápagos calderas. It has near vertical ring faults on all sides, except in the north, exposing 100–140 m of lava flows (Reynolds et al., 1995). The elevated central caldera floor is covered by aa flows that dip slightly to the east and is bounded to the west and south by an intra-caldera fault system consisting of outward dipping normal faults (Fig. 2). The fault scarps dip steeply outwards (60–90°) and are over 100 m high to the west, but lower to the south. The fault system in the western part of the caldera has a prominent sinuous ridge with lava flows on top that dip steeply eastward (20–60°) and then bend sharply to merge with the gently dipping (1–3°) central caldera floor (Reynolds et al., 1995). The sinuous ridge gradually becomes less prominent where its general trend changes from north–south to east–west orientation, until it disappears north of the southern intra-caldera faults (Fig. 2).

We mapped the location of faults within the southern part of the intra-caldera fault system on Sierra Negra volcano using a hand-held GPS instrument during fieldwork in 2001. The larger faults in the
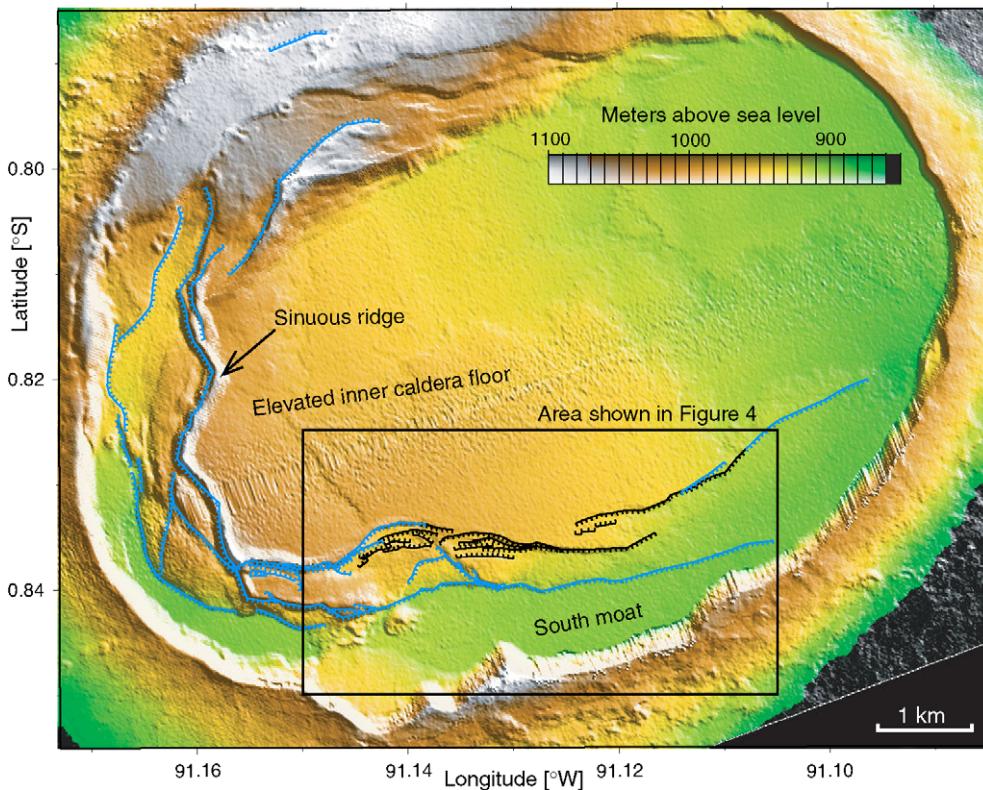
Fig. 2. TOPSAR topographic map of Sierra Negra caldera showing intra-caldera faults mapped in 2001. Faults in black were mapped in the field using GPS measurements and faults in blue were mapped directly from aerial photographs and a digital elevation model. The caldera ring faults are not shown as their location is obvious from the topography. Faults in the northern part of the caldera were not mapped. The rectangle marks the area shown in Fig. 4a–b.
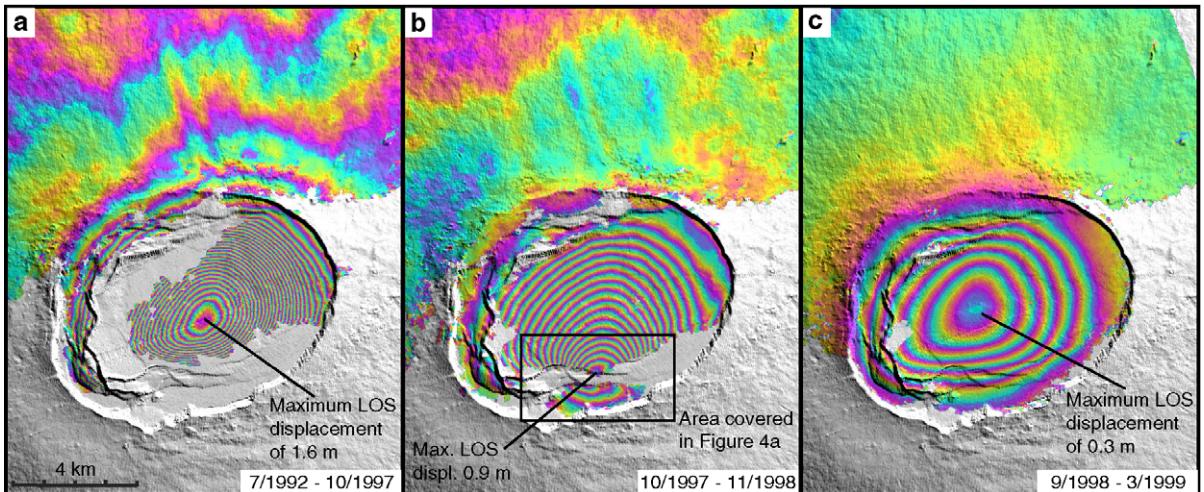
Fig. 3. Satellite radar interferograms of Sierra Negra caldera showing uplift during three time periods: (a) 1992–1997 (5.3 years, descending orbit), (b) 1997–1998 (1.1 years, descending orbit), and (c) 1998–1999 (0.5 years, ascending orbit). Each color cycle represents 5 cm line-of-sight (LOS) displacement up towards the satellites. The rectangle in (b) indicates the area shown in Fig. 4a.

west were mapped using aerial photographs and a TOPSAR digital elevation model (Zebker et al., 1992; Mouginis-Mark et al., 1996). The resulting fault map of the intra-caldera fault system is shown in Fig. 2. The southern part of the fault system is quite complex, with several parallel and overlapping south facing normal faults. Here, the total offset of each fault scarp is typically 0–20 m, increasing towards the west to about 100 m where the sinuous ridge bends sharply towards the north. Small grabens exist near some of the faults, illustrating the extensional regime under which these faults have formed.
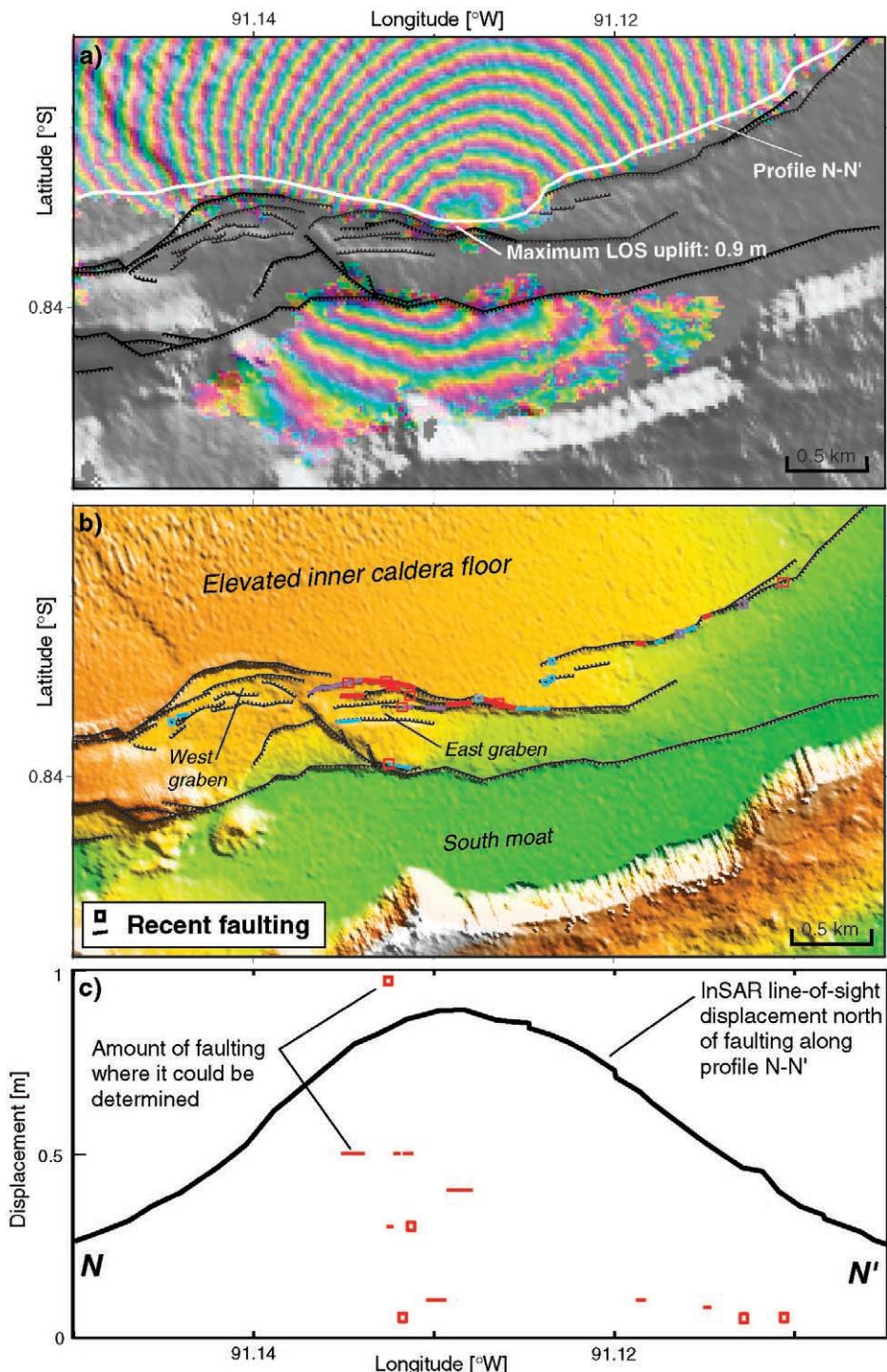
3. Review of observed volcano deformation 1992–2002

Little was known about the present-day crustal deformation on Galápagos volcanoes prior to our earlier studies (Jónsson et al., 1999; Amelung et al., 2000). We found that InSAR observations revealed time-varying uplift at most volcanoes in the western Galápagos during 1992–1999. The greatest uplift was observed on Sierra Negra volcano, up to 2.7 m, but it was both spatially and temporally variable during this time period. In 1992–1997 and 1998–1999 the uplift patterns were similar with the maximum uplift located at the center of the caldera (Fig. 3a and c). Inflation during 1997–1998, however, was markedly asymmetric with maximum uplift near the south rim of the caldera (Fig. 3b). Here, the interferometric phase is discontinuous across the south-facing normal faults that bound the elevated inner-caldera floor.

More recent InSAR data (not shown here) indicate that the caldera floor changed from inflation to deflation in Fall of 2001. Campaign GPS measurements, conducted on Sierra Negra since January 2000, also reveal this change from inflation to deflation. Maximum GPS uplift of 7 cm/year was observed between January 2000 and January 2001, but defla-

Fig. 4. Field evidence for recent faulting in comparison with the InSAR observations. (a) A blowup of the InSAR observations from 1997 to 1998 in the southern part of Sierra Negra caldera (here each color-cycle is 2.8 cm line-of-sight (LOS) displacement). The measurements are discontinuous across the faults and it is not possible to determine the absolute amount of offset across the faults from these data. (b) Localities where signs of recent faulting were found in the southern part of Sierra Negra caldera. Lines show where near continuous evidence was detected while squares show single localities where evidence was found. The colors indicate different classes of evidence (see text): 1—red, 2—purple, 3—cyan. (c) Amount of recent faulting at the few locations where it could be estimated in the field. The squares and lines show cumulative faulting estimates on parallel fault strands. InSAR LOS displacements north of the faults (see profile N–N′ in a), relative to a far-field zero, are shown in comparison to the field estimates.

tion of 11.5 cm/year was observed between January 2001 and May 2002 (Johnson et al., 2002). Six continuous GPS stations, installed in May 2002, showed continuing deflation at a rate of ~10 cm/year during the first 3 months of operation (Johnson et al., 2002). The magnitude of observed uplift and the high eruption frequency at Sierra Negra volcano suggest that the observed uplift was due to magma accumulation under the caldera. Pre-eruptive inflation and co-eruptive subsidence observed at the neighboring Cerro Azul volcano also suggest that the observed deformation at Galápagos calderas is of magmatic origin (Amelung et al., 2000).

To better understand the cause of uplift on Sierra Negra, we investigated several models simulating the observed deformation. The simplest model for volcanic inflation is perhaps the Mogi model, a point pressure source in an elastic half-space (Mogi, 1958). Simulated interferograms using a single Mogi source have fringe patterns that are nearly circularly symmetric and cannot reproduce the ovoid uplift patterns observed in 1992–1997 and in 1998–1999 at Sierra Negra (Fig. 3a and c; Amelung et al., 2000). Modeling uplift from a pressure increase within a finite prolate spheroidal cavity in an elastic halfspace (Yang et al., 1988) can produce an elliptical fringe pattern, but also does not closely match the observed deformation. A better fit to the observed deformation follows from a sill intrusion whose opening varies spatially. The optimal-fit sill depth was found to be around 2 km and for the 1998–1999 time period the increase in sill thickness was up to 0.5 m (Amelung et al., 2000). Note that the expanding magma body itself is probably much thicker as the data are only sensitive to the change in thickness.

The uplift pattern during 1997–1998 is very different from what was observed both before and after this period, with the maximum uplift located near the southern intra-caldera faults (Fig. 3b). The interferometric phase is discontinuous across the faults, but a small patch with coherent InSAR phase exists to the south, just north of the caldera rim (Figs. 3b and 4a). The phase gradient on the coherent patch shows tilt down towards the north, focused towards the uplift maximum just north of the faults, which suggests that faulting occurred across the south facing normal faults. However, it is not possible to determine the displacement of the patch

relative to the area north of the faults because the InSAR data are incoherent everywhere around the patch. When modeling the 1997–1998 data we used four fault patches representing the southern intra-caldera faults (Amelung et al., 2000). This model suggested that up to 1.2 m of displacement occurred across these faults.

4. Field evidence of recent faulting

In January 2001 we searched for field evidence of recent faulting along the southern part of the intra-caldera fault system at Sierra Negra (Fig. 2). The fieldwork consisted of walking along the different fault strands, mapping their locations and documenting any evidence suggestive of recent fault movement. It should be made clear that the southern intra-caldera faults did not form during the 1997–1998 episode; they're older with cumulative displacement of 10s of meters. Therefore, our aim was to identify fresh-looking surfaces at the base of these faults, which might indicate that faulting recently took place. Most of the area near the southern intra-caldera faults is covered by rough aa lava flows which makes this task difficult, as the bottom of exposed fault-walls is commonly covered with talus. In addition, the caldera is arid and the lavas are not much weathered, which makes recently emerged rocks hard to distinguish from other surface rocks. Furthermore, the sparse vegetation in the caldera, consisting mainly of dry ferns and moss, was of help at only few locations in identifying recent faulting. These circumstances made it difficult to identify and quantify recent faulting with confidence, and impossible to verify that it happened in 1997–1998.

Evidence for recent faulting was found at several locations, although most of the examined faults showed no evidence. We categorized our findings into three groups: (1) Clear evidence of faulting with continuous fresh fault surfaces and sometimes-quantifiable displacement. (2) Faulting suggested by some fresh fault surfaces, often discontinuous and usually not quantifiable displacement. (3) Indirect evidence of possible fault movement, such as fresh talus and overturned stones; features that could also be due to weathering. The locations where signs of recent faulting were found are shown in Fig. 4b and a

description of each case can be found in Jónsson (2002).

Most of the evidence for recent faulting was found within 1 km east and west of the line-of-sight (LOS) displacement maximum observed in the InSAR data (Fig. 4a–b). In some cases we found evidence for faulting on parallel strands of the fault system indicating that the near-surface faulting may have been distributed among several faults, rather than on only one fault. We found less evidence for recent faulting further east and west where less faulting is also indicated by the InSAR data. Some of the largest faults in the southwestern part of the caldera (Fig. 2, just west of the blowup shown in Fig. 4b) do not appear to have moved recently.

The amount of recent faulting could be measured at only a few locations, e.g., where sparse vegetation or moss could be matched across the rupture. In no case was this easily quantifiable as some 3 years had passed since the faulting took place (if it occurred in 1997–1998), thus, these estimates are not definite. Where faulting was quantified at parallel fault strands the values were added. The results are shown in Fig. 4c in comparison to the InSAR LOS displacement just north of the faults. Note that the LOS displacements do not show directly the amount of faulting, they only show by how much the northern wall moved up towards the satellites. The amount of faulting estimated in the field is generally smaller than the LOS displacements, however, the two maxima are co-located. It is not surprising that the amount of faulting, at the few locations it could be estimated, is smaller than the faulting inferred by the modeling as it is likely to be distributed across several faults.

In conclusion, we can say from our fieldwork that recent faulting occurred along the southern intra-caldera faults, perhaps sometime in 1997–1998. These observations indicate that the amount of faulting was at least 0.5–1 m, with maximum faulting co-located with the maximum InSAR LOS displacement.

5. SAR image offset measurements

The InSAR phase measurements are discontinuous across the intra-caldera faults, hence it is impossible to measure the fault offset directly from the interferogram (Fig. 4a). In our previous study the amount of faulting was estimated through modeling of the observed deformation (Amelung et al., 2000), as was discussed in Section 3. However, the radar data can be used to provide a direct measurement of the faulting, by comparing range offsets between pixels in two amplitude (backscatter) images (Fig. 5). The precision of such estimates is related to the radar resolution, rather than the fringe acuity.

Offset of features between two radar amplitude images (also referred to as SAR image offsets or pixel tracking) have in fact been used to measure ground displacements in large earthquakes (e.g., Michel et al., 1999; Peltzer et al., 1999; Jónsson et al., 2002) and can provide useful information about the location of the fault trace (Jónsson et al., 2002). But previous studies used only azimuth offset measurements; range offsets have usually been ignored. Azimuth offsets provide information about horizontal ground displacements parallel to the satellite flying direction that are perpendicular to the InSAR phase measurements. The range offsets, on the other hand, are sensitive to the same line-of-sight component as the more precise InSAR phase measurements, and therefore generally provide no extra information. Azimuth offset measurements are also more accurate than range offset measurements because the azimuth ground resolution is generally better (~4 m for the ERS satellites) than the range ground resolution (~20 m). Typically, we
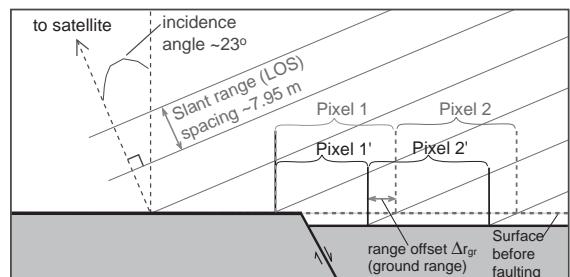
Fig. 5. Schematic figure showing how faulting can be detected by range offset measurements. Like InSAR observations, the range offsets are most sensitive to vertical movements (i.e., for ERS incidence angle of ~23°). In the radar image acquired before faulting occurs reflections from the ground map into range pixels 1 and 2, but into pixels 1′ and 2′ after the faulting. Cross-correlation between the two radar images gives the range offset. The slant range spacing of the ERS radars is 7.95 m, corresponding to roughly 20 m on the ground. The elevation change needed to cause ground range offset Δr_{gr} or slant range (LOS) offset Δr_{LOS} is therefore $\Delta h = \Delta r_{gr} \tan \theta = \Delta r_{LOS}/\cos \theta$, where θ is the incidence angle.

can measure pixel offsets locally between two images to 1/32 of a pixel, thus the accuracy of the azimuth offsets is 12.5 cm, but 62.5 cm for the range offsets (Jónsson et al., 2002). Sierra Negra volcano presents a case where range offsets are useful, despite the large uncertainties, as large vertical displacements occurred across the intra-caldera faults.

We measure range offsets at Sierra Negra volcano using two amplitude images, acquired in September 1997 and October 1998. The radar images are the same as those used to form the 1997–1998 interferogram (Fig. 3b). The range offsets are estimated locally by cross-correlation of 32×32 pixel sub-images. The resulting line-of-sight range offsets Δr_{LOS} are noisy with values ranging from negative 1–2 m to positive

1–2 m (Fig. 6a). East and west of the caldera the offset values are out of scale because sub-images there do not correlate well due to dense vegetation. Within the caldera the offset image has more positive values than negative values, indicating uplift towards the satellite relative to the area northwest of the caldera. To see this uplift better, we calculate the average range offset along a profile (boxes in Fig. 6a) and plot the averages from north to south in Fig. 6b. The averages show a clear range decrease (uplift towards the satellites) of the central caldera floor that becomes more prominent towards the south and agrees well with the InSAR data. The range offsets show a sharp 1.4 ± 0.2 m step across the southern intra-caldera faults, with range decrease of 0.9 ± 0.1 m observed just north of the
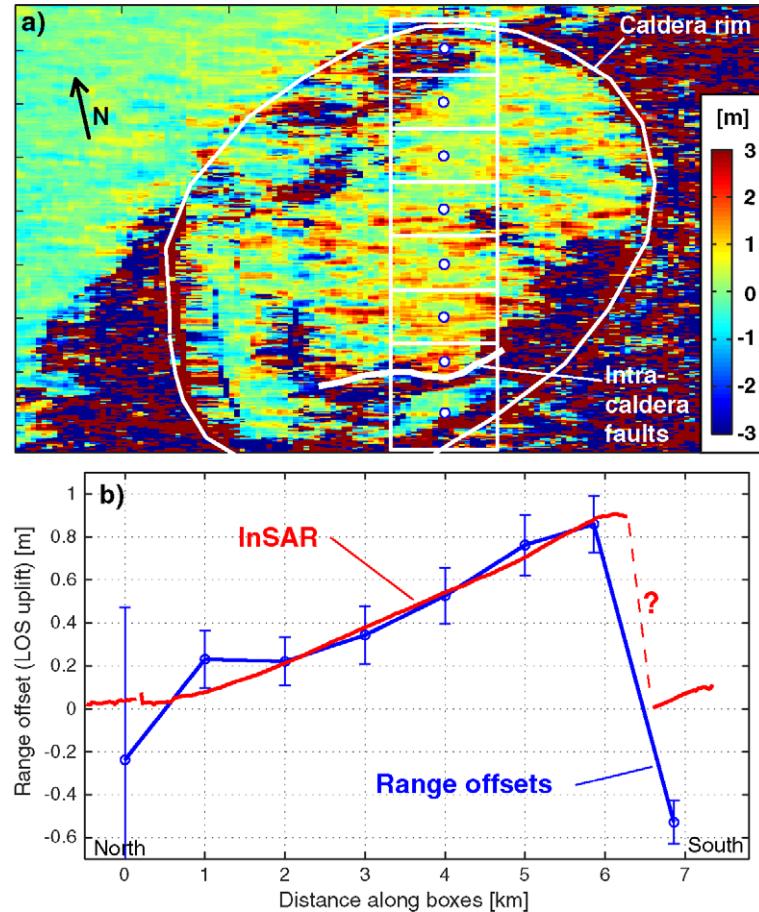
Fig. 6. SAR range offset measurements of Sierra Negra caldera. (a) Map showing slant range (LOS) offsets measured in the caldera during 1997–1998. Uplift into line-of-sight towards the satellite is shown positive. (b) Range offset averages from boxes shown in (a) from north to south in comparison to the InSAR data. The range offsets show 1.4 ± 0.2 m step across the southern intra-caldera faults.

faults and 0.5 ± 0.1 m range increase observed just south of the faults (Fig. 6). Note that even though the range offsets are discontinuous across the faults, the measurements are not ambiguous as is the case for the conventional InSAR phase measurements.

Azimuth offset measurements of Sierra Negra volcano during the same time period (not shown here) do not show large displacements, indicating that the ground motion was primarily vertical. If we assume that vertical ground motion was responsible for observed range offsets at Sierra Negra, we can infer the amount of vertical displacements Δh needed to produce the observed offsets: $\Delta h = \Delta r_{\mathrm{LOS}}/\cos\theta$, where Δr_{LOS} is the measured offset in the line-of-sight (LOS) direction and θ is the incidence angle (Fig. 5). This implies that the observed range offset of 1.4 ± 0.2 m corresponds to vertical displacement across the faults of 1.5 ± 0.2 m. This direct estimate of the intra-caldera faulting from the range offsets is a bit larger than what we estimated in the field. However, the field observations (0.5–1 m) only provided a minimum estimate of the maximum faulting, so we believe that the range offset estimate (1.5 ± 0.2 m) is more reliable. Our previous modeling result based on the InSAR data alone had up to 1.2 m of faulting (Amelung et al., 2000), which agrees with range offset estimate at a 95% confidence interval.

6. Discussion

The results of the fieldwork and the range offset measurements clearly support our previous interpretation of the InSAR data that trapdoor faulting took place within the caldera of Sierra Negra volcano. In this section we begin by examining why trapdoor faulting occurs at Sierra Negra, we then estimate the current total thickness of the intrusion underneath the caldera floor, and finally we discuss what the observed processes tell us about longer-term behavior of Sierra Negra volcano.

6.1. Conditions of trapdoor faulting

The strong uplift prior to 1997, which we have modeled by an inflating sill at ~2 km depth beneath the caldera floor (Amelung et al., 2000), seems to have led to trapdoor faulting sometime in 1997–1998. The inferred presence of a sill intrusion indicates that the minimum compressional stress is vertical and that reverse faulting is favored. Such stress regime does not explain why the trapdoor faulting occurs. However, the faults are located near the peripheries of the intrusion, which suggests that the sill growth plays a major role in triggering the faulting.

The mechanism of growth of sills and laccolithic intrusions has been studied by several authors (e.g., Johnson and Pollard, 1973; Pollard and Johnson, 1973; Gudmundsson, 1990; Fialko, 2001). Results of two-dimensional elastic boundary element modeling by Fialko (2001) of propagating sill intrusions (treated as a fluid-pressurized cracks in elastic half-space) provide insights into the processes observed at Sierra Negra. These results show that when the lateral extent (half-length) of an intruding sill becomes comparable to and exceeds its depth, the intrusion will increasingly start to interact with the free surface with deformation concentrating above the intrusion and with the sill starting to propagate towards the surface. The resulting stress concentrations in the intrusion roof, when the sill begins to bend up towards the surface, can lead to faulting on outward-dipping or nearly vertical normal faults, given sufficiently high excess magma pressures (Fialko, 2001). The dimensions of Sierra Negra are consistent with this model with our estimated sill depth of ~2 km and faulting occurring ~3 km south of the sill center (Fig. 7a–b). Observations by Johnson and Pollard (1973) of diorite laccolith intrusions in Henry Mountains, Utah, also support this. They found intrusion host rocks to be especially deformed over the peripheries of the laccoliths and reported that laccoliths terminate abruptly, e.g., against a nearly vertical fault or by a peripheral dike cutting upward through the host rock. Therefore, our interpretation that the observed faulting at Sierra Negra is caused by a growing sill intrusion is supported both by results of numerical modeling and field observations of eroded intrusions.

6.2. Intrusion thickness

Another important question is what is the thickness of the sill intrusion at Sierra Negra. The uplift observed during 1992–1999 is consistent with a sill
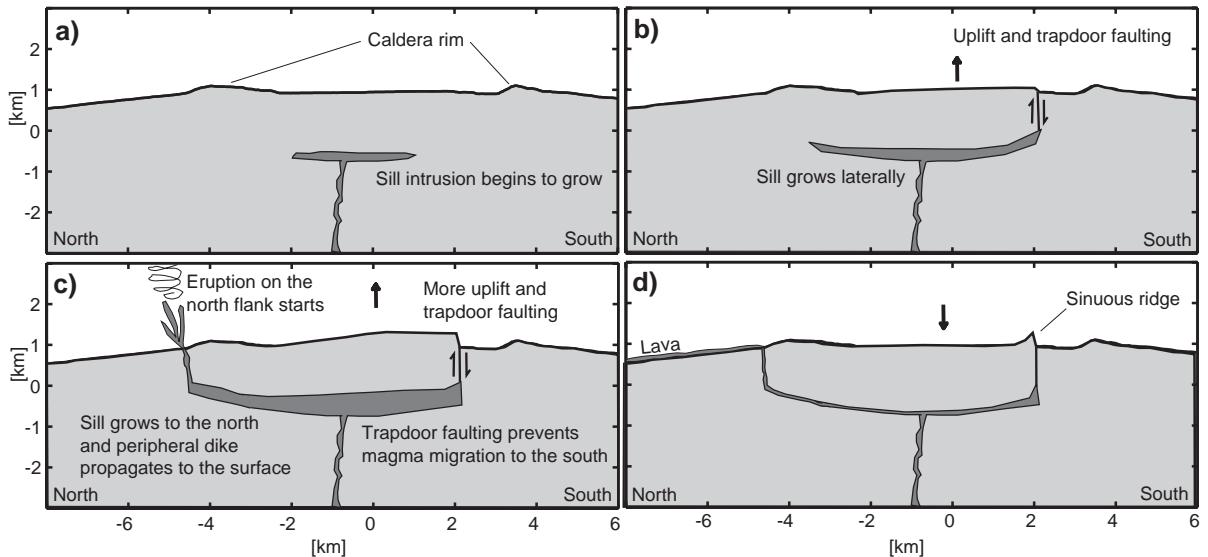
Fig. 7. Schematic diagrams showing magma accumulation and faulting at Sierra Negra in a N–S cross-section across the caldera. Sub-figures a–b represent recent evolution at Sierra Negra, while c–d represent hypothetical future evolution with a formation of a ridge, similar to the sinuous ridge in the western part of the caldera. (a) A sill intrusion begins to grow under the central caldera floor. (b) The sill grows laterally causing trapdoor faulting on the southern intra-caldera faults. (c) If magma influx resumes in the future it probably will cause further uplift and trapdoor faulting. The faulting will probably prevent sill growth to the south but sill propagation to the north might lead to an eruption on the north flank through a peripheral dike. (d) After a large eruption the caldera floor will deflate and might leave a ridge structure in the south. The caldera topography and sill depth are drawn at the correct scale in a, but the sill thickness, the sinuous ridge, amount of uplift and faulting are exaggerated in subsequent figures.

intrusion with a radius of ~3 km whose thickness increased by up to 4 m. However, the data do not provide information about the total thickness of the intrusion. This uplift episode at Sierra Negra probably started following the last eruption in 1979, but no data exist for the time period 1979–1992. The uplift rate of basaltic volcanoes is often the fastest just after eruptions and then slows down with time. Good examples of this uplift pattern have been observed at Krafla volcano in Iceland (Björnsson, 1985) and at Kilauea in Hawaii (Dvorak and Dzurisin, 1997). This pattern of uplift was also observed after the 1998 eruption of Cerro Azul, which is located 30 km southwest of Sierra Negra. However, the uplift rate at Sierra Negra was slower during 1992–1997 (0.32 m/year) than during 1998–1999 (0.65 m/year), so Sierra Negra seems to have been following a different uplift pattern.

The thickness of the intrusion can be estimated for given magma overpressure if we approximate it as a finite circular crack in an infinite elastic body. The maximum half-width $w_{\max}^{\mathrm{sill}}$ of such a sill is linearly related to the overpressure Δp_{v} and radius a (e.g., Pollard and Johnson, 1973):

$$w_{\max}^{\mathrm{sill}} = \frac{2\Delta p_{\mathrm{v}} a}{\pi \mu}(1 - v) \qquad (1)$$

where μ is shear modulus and v Poisson's ratio. For radius of 3 km and sill thickness of $2w_{\max}^{\mathrm{sill}}=4$ m the predicted magma overpressure is 14–21 MPa (using μ=10–15 GPa and v=0.25), which is high, but maybe not impossible. However, a model of a sill embedded in an full elastic body is not the right model for Sierra Negra, as the intrusion radius exceeds the intrusion depth d (i.e., a/d>1). In these cases the intrusion is likely to start bending the overburden layers resulting in increasing thickness to radius ratio (Gudmundsson, 1990), and the sill will grow into a laccolith intrusion. The transition from a circular sill to a laccolith has been estimated to occur when a/d_{e}=1.9, where d_{e} is the "effective" thickness of the overburden layers (Pollard and Johnson, 1973). Effective thickness is the thickness of a single layer which has the same resistance to bending as the stack of the overburden

layers, and is therefore smaller than the total thickness of the stack. More careful analysis of the transition from a sill to a laccolith indicates that it may happen for a/d_e ratios even smaller than 1 (Pollard and Holzhausen, 1979). The caldera floor on Sierra Negra is probably made up by multiple lava flows. The caldera ring faults expose 100–140 m of lava flows and the western intra-caldera faults some 100 m as well (Reynolds et al., 1995). Using effective thickness of $d_e=0.3d$, which has been estimated for basaltic lava piles in Iceland (Gudmundsson, 1986) and used for oceanic crust (Gudmundsson, 1990), the intrusion at Sierra Negra has a/d_e ratio of ~5. Therefore, it is more appropriate to call the intrusion at Sierra Negra a laccolith, rather than a sill.

The maximum thickness of the laccolith grows proportional to the fourth power of its radius (Pollard and Johnson, 1973), which is very different from the simple sill described above whose thickness grows only linearly with increasing sill radius. Here, the maximum deflection w_{max}^{lacc} of overburden layers with effective thickness of d_e, due to a circular laccolith with radius a and uniform magma overpressure of Δp_v is (Pollard and Johnson, 1973):

$$w_{max}^{lacc} = \frac{3\Delta p_v a^4}{32\mu d_e^3}(1-v). \qquad (2)$$

Maximum deflection of 4 m and intrusion radius of 3 km results in magma overpressure of only 1–2 MPa. This indicates that the intrusion is thicker as it has already reached a radius of 3 km. A more reasonable magma overpressure of 5–10 MPa results in maximum laccolith thickness of ~10–30 m. The volume of such a laccolith is 0.2–0.6 km³, assuming the average thickness represents 2/3 of the maximum thickness. This volume estimate is somewhat smaller than the estimated volume (0.9 km³) of the 1979 eruption (Reynolds et al., 1995). However, one should bear in mind that this volume estimate is very sensitive to small changes of some estimated parameters, such as the radius of the intrusion and the effective thickness of the overburden layers. For example, an intrusion radius of 3.6 km, instead of 3 km, will double this volume estimate, and using $d_e=0.4d$ (instead of $d_e=0.3d$) will reduce it by a half. Therefore, we conclude by pointing out that the estimated 4 m thickening of the intrusion during 1992–1999 is not representative of the total thickness, and that the intrusion is likely to be considerably thicker.

6.3. Longer-term evolution of Sierra Negra

Recent observations indicate that magma influx to the Sierra Negra intrusion stopped in 2001. If magma influx resumes it will result in continuing uplift and further trapdoor faulting. The intra-caldera faulting probably prevents magma propagation to the south, although northward magma migration is likely with growing intrusion thickness. This propagation may eventually lead to a eruption on the north flank, as has happened repeatedly in the past, most recently in 1979. The propagating sill model of Fialko (2001) predicts that after the intrusion starts to bend upwards it may find its way to the surface and initiate an eruption at a distance about 3 times the sill depth. This is consistent with the dimensions at Sierra Negra where eruptive fissures on the north flank exist at distances 5–6 km north of the sill center. However, there appear to be at least two problems with this comparison. First, the laccolith model predicts that the deflection of the overburden layers grows as the forth power of the intrusion radius and it would predict a laccolith thickness of 100s of meters before its areal extent reaches the north flank. Second, the propagating sill model predicts that the sill cuts the surface under a shallow angle (Fialko, 2001, Fig. 2), while the eruptive vents on the north flank indicate that the feeding dikes were steep (William W. Chadwick, personal communication, 2004). The first problem can be circumvented by simply adjusting parameters in the laccolith model, e.g., by increasing the effective thickness of the overburden layers. The second problem may indicate that intrusions in the past did not gradually ascend to the surface, but terminate abruptly with a peripheral dike cutting vertically upward through the host rocks (Fig. 7c), as has been observed at eroded laccoliths (Johnson and Pollard, 1973).

The previous reasoning raises the question about why the growing intrusion results in trapdoor faulting inside the caldera instead of a peripheral dike cutting upwards to the surface, like what may have happened on the north flank. Pollard and Johnson (1973) discuss this issue and conclude that for faulting to be favored above a peripheral dike, a significant part of the stack must have been weakened by fracturing. Intra-caldera

collapses exist within some of the other Galápagos calderas and their ring faults present an example of intra-caldera weaknesses. Therefore, it is not impossible that the trapdoor faulting at Sierra Negra reactivated old ring faults that had been submerged by later caldera lava flows, although we do not have any evidence for old intra-caldera ring faults at Sierra Negra. In any case, this brings up another question on what may be the fault dip of the intra-caldera faults? In the western part of the caldera, where these faults are the most prominent, the fault scarps have an outward dip of 60–90° (Reynolds et al., 1995). This observation, however, may not represent the fault dip at depth as these fault scarps make up the sinuous ridge that is heavily tilted. The newer and much smaller fault scarps along the southern part of the intra-caldera faults system appear vertical. As discussed above, the propagating sill model predicts that faulting might occur at outward dipping or nearly vertical faults, as the sill starts to bend upwards (Fialko, 2001). In addition, the observations of Johnson and Pollard (1973) demonstrated that laccoliths sometimes terminate at a vertical fault. Therefore, given these results of numerical modeling and field observations, as well as the requirement of pre-existing weakness for the faulting to occur, we conclude that the intra-caldera faults are probably nearly vertical at depth.

The height of the intra-caldera fault system indicates that trapdoor faulting must have occurred repeatedly in the past to form the fault scarps that are up to 100 m high along parts of the sinuous ridge (Fig. 2). The lava flows that fill the caldera are 1000–3000 years old (Reynolds et al., 1995), which provides an upper bound on the age of the surface faults, although the fault system may be older. The sinuous ridge has steeply dipping lava flows on top that sharply bend to merge with the gently dipping caldera floor (Reynolds et al., 1995). The fault scarp along the ridge are 60–80 m higher than the central caldera floor that it bounds. This implies that the elevated intra-caldera floor stood much higher at the time the western faults formed, but has since subsided considerably, probably due to voluminous magma withdrawal from a shallow reservoir, possibly to fissure eruptions on the north flank. During subsidence the fault system is put under compression, preventing the faults from 'slipping back', resulting in the ridge formation when the central floor becomes lower than the faults (Fig. 7d). This explanation for the formation of the sinuous ridge is similar to the one provided by Reynolds et al. (1995). Their preferred explanation is that incremental subsidence of the caldera floor, after initial uplift, "resulted in the rigid floor becoming jammed along its western and northern edges where it broke rigidly in several places and formed the unusual blocks that make up the sinuous ridge" (Reynolds et al., 1995). Although we believe that the uplift was incremental and the subsidence with the ridge formation relatively fast, the two explanations for the formation of the sinuous ridge are essentially the same.

If the interpretation of the formation of the sinuous ridge is correct, it indicates that the magma intrusion was 60–80 m thicker at the time when the caldera floor was at its highest position, than it is today. A sill that has a radius of 3–4 km and maximum thickness of ~100 m would represent a volume of 2–3 km^3 (assuming that the average thickness is 2/3 of the maximum thickness). This volume is somewhat larger, but comparable to, the volume estimate of the 1979 lava of 0.9 km^3 (Reynolds et al., 1995). However, there is no reason to assume that the highest position of the caldera floor was reached before the last eruption as the high western intra-caldera faults are probably much older.

7. Conclusions

Field observations at Sierra Negra volcano in 2001 indicate that recent faulting occurred along the southern intra-caldera faults, perhaps sometime in 1997–1998. The maximum amount of faulting estimated in the field is at least 0.5–1 m. Range offset measurements of radar amplitude images show 1.4±0.2 m line-of-sight displacement across the southern intra-caldera faults in 1997–1998. This indicates that 1.5±0.2 m of faulting occurred, assuming vertical displacements. Trapdoor faulting at Sierra Negra is likely caused by excess magma pressure in a shallow (~2 km) intrusion whose lateral extent (half-length) has become greater (~3 km) than its depth. Although the uplift observed during 1992–1999 can be simulated using a sill that has a maximum thickness of ~4 m, the total thickness of the intrusion is likely to be on the order of 10–30 m. The volume of such an

intrusion is 0.2–0.6 km^3, a bit smaller, but comparable to, the volume erupted in the 1979 eruption.

Acknowledgments

References

Amelung, F., Jónsson, S., Zebker, H., Segall, P., 2000. Widespread uplift and 'trapdoor' faulting on Galápagos volcanoes observed with radar interferometry. Nature 407, 993–996.

Björnsson, A., 1985. Dynamics of crustal rifting in NE Iceland. J. Geophys. Res. 90, 10151–10162.

Chadwick Jr., W.W., Dieterich, J.H., 1995. Mechanical modeling of circumferential and radial dike intrusion on Galapagos volcanoes. J. Volcanol. Geotherm. Res. 66, 37–52.

Chadwick Jr., W.W., Howard, K.A., 1991. The pattern of circumferential and radial eruptive fissures on the volcanoes of Fernandina and Isabela islands, Galapagos. Bull. Volcanol. 53, 259–275.

Christie, D.M., Duncan, R.A., McBirney, A.R., Richards, M.A., White, W.M., Harpp, K.S., Fox, C.G., 1992. Drowned islands downstream from the Galapagos hotspot imply extended speciation times. Nature 355, 246–248.

Dvorak, J.J., Dzurisin, D., 1997. Volcano geodesy: the search for magma reservoirs and the formation of eruptive vents. Rev. Geophys. 35, 343–384.

Fialko, Y., 2001. On origin of near-axis volcanism and faulting at fast spreading mid-ocean ridges. Earth Planet. Sci. Lett. 190, 31–39.

Gudmundsson, A., 1986. Mechanical aspects of postglacial volcanism and tectonics of the Reykjanes peninsula, southwest Iceland. J. Geophys. Res. 91, 12711–12721.

Gudmundsson, A., 1990. Emplacement of dikes, sills and crustal magma chambers at divergent plate boundaries. Tectonophysics 176, 257–275.

Johnson, A.M., Pollard, D.D., 1973. Mechanics of growth of some laccolithic intrusions in the Henry Mountains, Utah: I. Field observations, Gilbert's model, physical properties and flow of the magma. Tectonophysics 18, 261–309.

Johnson, D., Geist, D., Chadwick, D., 2002. A change from inflation to deflation at Sierra Negra volcano, Galapagos revealed by GPS and gravity monitoring. Eos Trans. AGU 83 (47), Fall Meet. Suppl. Abstract T11E-06.

Jónsson, S., 2002. Modeling volcano and earthquake deformation from satellite radar interferometric observations. PhD thesis, Stanford University, 164 pp.

Jónsson, S., Zebker, H., Cervelli, P., Segall, P., Garbeil, H., Mouginis-Mark, P., Rowland, S., 1999. A shallow-dipping dike fed the 1995 flank eruption at Fernandina volcano, Galápagos, observed by satellite radar interferometry. Geophys. Res. Lett. 26, 1077–1080.

Jónsson, S., Zebker, H., Segall, S., Amelung, F., 2002. Fault slip distribution of the 1999 M_w7.1 Hector Mine, California, earthquake, estimated from satellite radar and GPS measurements. Bull. Seismol. Soc. Am. 92, 1377–1389.

Michel, R., Avouac, J.-P., Taboury, J., 1999. Measuring ground displacements from SAR amplitude images: application to the Landers earthquake. Geophys. Res. Lett. 26, 875–878.

Mogi, K., 1958. Relations between the eruptions of various volcanoes and the deformation of the ground surface around them. Bull. Earthq. Res. Inst. Univ. Tokyo 36, 99–134.

Mouginis-Mark, P.J., Rowland, S.K., Garbeil, H., 1996. Slopes of western Galápagos volcanoes from airborne interferometric radar. Geophys. Res. Lett. 23, 3767–3770.

Munro, D.C., Rowland, S.K., 1996. Caldera morphology in the western Galápagos and implications for volcano eruptive behavior and mechanisms of caldera formation. J. Volcanol. Geotherm. Res. 72, 85–100.

Peltzer, G., Crampé, F., King, G., 1999. Evidence of nonlinear elasticity of the crust from the Mw7.6 Manyi (Tibet) earthquake. Science 286, 272–276.

Pollard, D.D., Holzhausen, G., 1979. On the mechanical interaction between a fluid-filled fracture and the earth's surface. Tectonophysics 53, 27–57.

Pollard, D.D., Johnson, A.M., 1973. Mechanics of growth of some laccolithic intrusions in the Henry Mountains, Utah: II. Bending and failure of overburden layers and sill formation. Tectonophysics 18, 311–354.

Reynolds, R.W., Geist, D., Kurz, M.D., 1995. Physical volcanology and structural development of Sierra Negra volcano, Isabela island, Galápagos archipelago. Geol. Soc. Am. Bull. 107, 1398–1410.

Simkin, T., Siebert, L., 1994. Volcanoes of the World, 2nd edition. Geoscience Press, Tucson, 349 pp.

Yang, X.-M., Davis, P.M., Dieterich, J.H., 1988. Deformation from inflation of a dipping finite prolate spheroid in an elastic half-space as a model for volcanic stressing. J. Geophys. Res. 93, 4249–4257.

Zebker, H.A., Madsen, S.N., Martin, J., Wheeler, K.B., Miller, T., Lou, Y., Alberti, G., Vetrella, S., Cucci, A., 1992. The TOPSAR interferometric radar topographic mapping instrument. IEEE Trans. Geosci. Remote Sens. 30, 933–940.